A R C H I V E S O F M E T A L L U R G Y A N D M A T E R I A L S
Volume 53 2008 Issue 1

A. BACZMAŃSKI*, R. DAKHLAOUI**, C. BRAHAM**, K. WIERZBANOWSKI*

EXAMINATION OF MECHANICAL BEHAVIOUR OF AGED DUPLEX STEEL USING X-RAY AND NEUTRON DIFFRACTION METHODS

BADANIE WŁASNOŚCI MECHANICZNYCH STALI DWU-FAZOWEJ PODDANEJ STARZENIU PRZY UŻYCIU DYFRAKCJI RENTGENOWSKIEJ I NEUTRONOWEJ

The parameters characterizing the elastoplastic mechanical behaviour of each phase in austeno-ferritic duplex stainless steels were determined using X-ray and neutron diffraction during a uniaxial tensile test. The elastoplastic self-consistent model was used to predict the evolution of the lattice elastic strains during loading and to identify the critical resolved shear stresses and work hardening parameters of the material. The effect of ageing treatment on the elastoplastic behaviour of both phases was also studied. It was found that thermal ageing of austeno-ferritic steel caused microstructural transformations and consequently a significant increase of the hardness of ferrite, while the mechanical properties of austenite remained practically unchanged.
Keywords: X-ray and neutron diffraction; phase stresses; duplex stainless steels; self-consistent model, thermal ageing

Parametry opisujące własności sprężysto-plastyczne każdej z faz w nierdzewnej stali austeno-ferrytycznej zostały wyznaczone przy użyciu dyfrakcji rentgenowskiej i neutronowej podczas testu rozciągania *in situ*. Zastosowano sprężysto-plastyczny model samo-uzgodniony do przewidywania sprężystych odkształceń sieci podczas próby rozciągania oraz do wyznaczenia krytycznych naprężeń ścinających na płaszczyznach poślizgu i parametrów umocnienia materiału. Zbadano również efekt wpływ starzenia na własności sprężysto-plastyczne obu faz. Stwierdzono, że proces termicznego starzenia stali austeno-ferrytycznej spowodował transformacje mikrostrukturalne i w konsekwencji wyraźny wzrost twardości ferrytu, podczas gdy własności mechaniczne austenitu pozostały praktycznie niezmienione.

1. Introduction

The hardening of austeno-ferritic duplex stainless steel can be caused by a reduction of the grain size, by solid solution (addition of nitrogen – an austenite stabilizing element, for example) or by precipitation of a number of intermetallics and other phases (such as σ phase, carbides or nitrides...). The size of grains in the austeno-ferritic steel is smaller than that of grains in the austenitic and in the ferritic steels. Thus, the Hall-Petch law predicts a larger hardness for the duplex steel than for the single-phase ferrite or austenite. Furthermore, phase boundaries play a considerable role in the hardening of duplex steel.

The thermal ageing of austeno-ferritic steels at temperatures lower than 600°C is characterised by microstructural transformations mainly in the ferritic phase. These transformations lead to a hardening of the ferrite and a subsequent loss of the impact toughness of the material [1]. Transformations in ferrite are mainly α/α' decomposition into Cr-poor α and Cr-rich α' domains and the precipitation of an intermetallic phase rich in Ni, Si and Mo (the G phase) [2-5]. The role of α' and the G phases in hardening and embrittlement of ferrite is widely discussed in the literature and the majority of authors agree that hardening is attributed essentially to the α' phase (see [6, 7] for example). Indeed, the coherence shift between the lattice parameters of α and α' phases introduces internal stresses reducing the mobility of dislocations. Moreover, α and α' have different Young modulus, what modifies energy necessary for the dislocation movement.

The G particles have very small size (between 1 and 10 nm generally and up to 50 nm occasionally) and they precipitate, more or less uniformly, in the ferritic grains depending on the chemical composition of

* FACULTY OF PHYSICS AND APPLIED COMPUTER SCIENCE, AGH- UNIVERSITY OF SCIENCE AND TECHNOLOGY, 30-059 KRAKÓW, 30 MICKIEWICZA AV., POLAND
** LIM, CNRS UMR 8006, ECOLE NATIONALE SUPERIEURE D'ARTS ET METIERS, 151 BD DE L'HOPITAL, 75013 PARIS, FRANCE

steel. The largest particles are formed preferentially in defects, the others are formed in the α/α' and $\gamma - \alpha$ interfaces. Their composition depends not only on the chemical composition of steel but also on the conditions of ageing. Other precipitations can also appear during the ageing for very long duration, like the $M_{23}C_6$ carbide precipitation and the secondary austenite γ_2 within ferrite. Some microstructural transformations can be present in the austenitic phase but they do not change mechanical properties of the material.

The α/α' decomposition of ferrite occurs according to two different mechanisms depending on the chromium content and on the temperature [5], i.e., spinodal decomposition ($280 \leqslant T \leqslant 475°C$) or nucleation and growth (often at 500°C). The α' and α phases have the same crystal structure (b.c.c.) with very similar lattice parameter (parameter of α' lattice is between those of iron and of chromium lattice). The α' phase can to contain up to 80% of chromium.

These microstructural transformations in ferrite are not visible in optical microscopy, nor in Scanning Electron Microscope (SEM), nor even by X-Ray diffraction. Resulting phases, being of nanometric size and of very close crystallographic structures, can be studied only by finer techniques such as Transmission Electron Microscope (TEM), Mössbauer spectroscopy or Small Angle Neutron Scattering (SANS).

The elastoplastic and the thermoelastic properties of duplex steel were investigated applying X-ray diffraction [8, 9], neutron diffraction [10, 11], FEM calculations [12, 13] and the self-consistent model [9-11]. In the present work, the neutron and X-ray diffraction methods were applied for "in situ" loaded duplex steel sample in order to compare elastoplastic behaviour of austenite and ferrite phases. The advantage of these methods is that the elastic strains can be measured separately in each phase and the experimental results can be directly compared with the self-consistent model. In order to find out the differences between both phases, the changes of interplanar spacings as a function of applied stress are studied. The effective parameters of plastic deformation are determined individually for ferrite and austenite [9-11]. The main purpose of this work is to observe the effect of ageing on mechanical behaviour of the phases in the studied duplex stainless steel.

2. Material and samples preparation

The studied material is an austeno-ferritic stainless steel, containing approximately 50% austenite and 50% ferrite. It was obtained by continuous casting, and then hot rolling down to 15 mm sheet thickness. The chemical composition of the alloy is given in Table 1. The characteristic microstructure of the steel consists of austenitic islands elongated along the rolling direction and embedded in a ferritic matrix (Fig. 1).

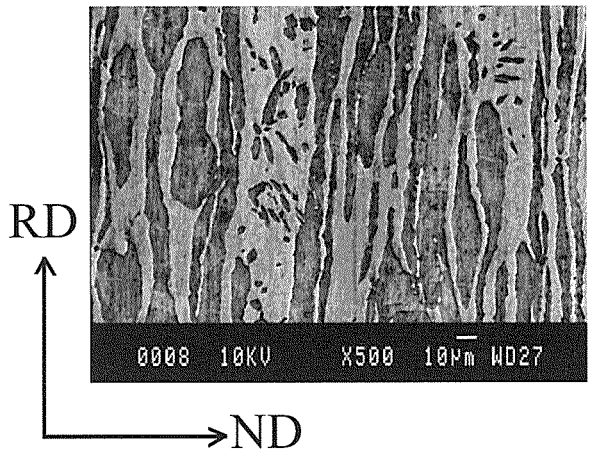

Fig. 1. Microstructure by scanning electron microscope shows islands of austenite (dark) in the ferrite matrix (light). The directions characteristic for rolling process are shown: RD-rolling direction, and ND-normal direction (TD-transfere direction is perpendicular to the sample surface)

For the first sample, a solution annealing heat treatment at 1050°C was given, followed by quenching in water in order to avoid the precipitation of secondary phases. The mechanical properties of this sample was already studied using X-ray [9] and neutron diffraction [10, 11]. In this work the second sample was prepared to study the effect of ageing treatment on the mechanical properties of ferrite and austenite. The temperature of ageing ($T<475°C$), in which only the decomposition of ferrite (into α and α' phases) by the mechanism of spinodal decomposition occurs, was chosen [2-5, 14]. Conditions of ageing were established according to the "TTP" diagram of duplex stainless steel [5, 15], i.e., the sample was annealed during 1000 hours at the temperature of 400°C and next cooled in the air.

TABLE 1
Chemical composition of duplex stainless steel X2 Cr Ni Mo 22.5.3 (UR45N): mass-percentage

C	Mn	Cr	Ni	Mo	Cu	S	N	Fe
0.015	1.6	22.4	5.4	2.9	0.12	0.001	0.17	balance

As shown in Table 1, the studied austeno-ferritic steel contains molybdenum. This alloy element favours both the α/α' decomposition and the G phase formation. Indeed, molybdenum is placed rather in the phase α' that in the phase α during decomposition process [16]. This creates additional stresses between α and α' and thus an additional hardening is obtained [16]. The presence of molybdenum in ferrite causes a reduction in solubility of nickel and thus silicon and nickel saturation. This supports the formation of G phase [17].

In addition to the precipitation of the G phase in dislocations and in the α/α' boundaries, controlled by the spinodal decomposition, other phenomena of embrittlement depending on the composition of austeno-ferritic steel and on the conditions of ageing can appear. The most frequently quoted precipitates are the carbides $M_{23}C_6$, nitrides (Cr_2N, π) and the secondary austenite γ_2. These precipitates influence considerably the mechanical properties and the corrosion resistance of the austeno-ferritic duplex steels [5, 18]. UR45N duplex steel studied in this work is not sensitive to the carbide formation because of molybdenum content. Molybdenum traps carbon and prevents it from diffusing in the ferrite/austenite interfaces [19]. Moreover, $M_{23}C_6$ carbides precipitate at sufficiently high temperatures ($\geqslant$500°C). Also, the nitrides and the secondary austenite γ_2 appear for temperatures of ageing quite higher than 400°C [5].

In conclusion, the microstructural mechanisms dominating for the chosen conditions in the studied austeno-ferritic steel (UR45N), are the spinodal decomposition of ferrite into α and α' phases accompanied by a precipitation of G phase in a very small quantity.

To check the occurrence of a precipitation of phases which could be detected by XRD, a $\theta/2\theta$ scan was carried out on aged austeno-ferritic steel, using a cobalt anticathode (λ_{Co} = 0.176 nm) (Fig 2). As shown in the diffractogram, apart from austenite and ferrite, no precipitation of secondary phases was detected by XRD. The α and α' phases of ferrite having very nearby lattice parameters (the difference between their lattice parameters is about 0,002 nm [18]) can not be separated from the diffractogram. Thus, only the average mechanical properties for both ferrite phases (α/α') are determined in this work using diffraction methods.

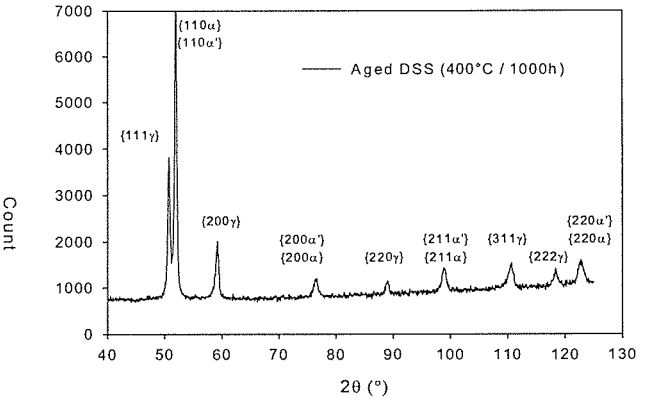

Fig. 2. Diffractogram for the aged stainless steel (X-rays, λ_{Co} = 0.176 nm)

3. Experimental techniques

Due to the hot rolling process both studied phases are significantly textured. The measurement of texture is of primary importance, because the quantitative information about the grain orientation distribution is essential for the elastoplastic deformation modelling as well as for the anisotropic diffraction elastic constants calculation [20-24]. By using X-ray diffraction on a Seifert diffractometer (LIM in ENSAM Paris), the experimental pole figures {111}, {200}, {110} and {200}, {220}, {211} were determined for the austenitic and the ferritic phases, respectively (the orientation of the sample coordinate system with respect to main directions of rolling is shown in Fig. 3a). Next, by using the WIMV algorithm [25], the orientation distribution functions (ODF, see [26]) were calculated from the experimental pole figures, independently for each phase (Fig. 4).

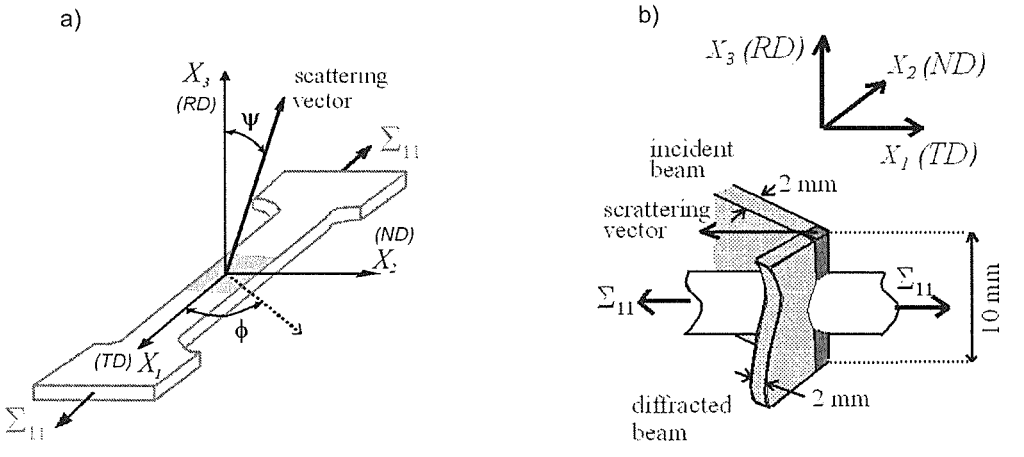

Fig. 3. Orientation of the sample with respect to the scattering vector and to the applied Σ_{11} stress during X-ray (a) and neutron (b) diffraction. In the case of X-ray measurements the direction of the scattering vector is variable and it is described by ϕ and Ψ angles

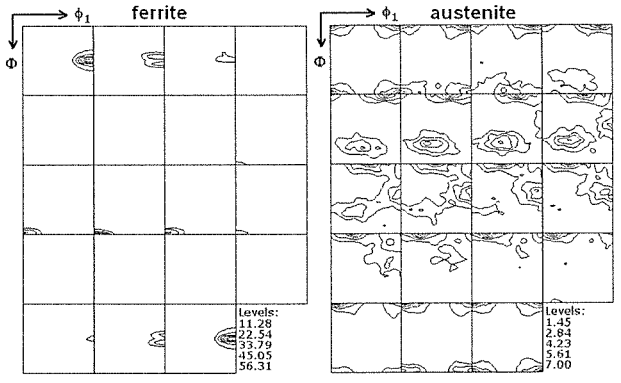

Fig. 4. Orientation distribution function (ODF) for both phases of duplex steel determined by X-ray diffraction. The sections through Euler space with a step of 5° along ϕ_2 axis are presented for austenite and ferrite phases (the sample frame is defined as: x_1||TD, x_2||ND and x_3||RD, cf. Fig. 3)

The $\sin^2\Psi$ X-ray diffraction method [23, 24, 27] was used to determine the phase stresses in the initial and in the "in situ" loaded samples. This method is based on the measurement of peak positions for a given hkl reflection and for various directions of the scattering vector, described by Ψ and ϕ angles [27] (see Fig. 3a).

The interplanar spacings in the austenite (311 reflection) were measured using manganese radiation ($\lambda_{K\alpha}^{Mn}$ = 0.21035 nm), while chromium radiation ($\lambda_{K\alpha}^{Cr}$ = 0.22911 nm) was used for the 211 reflection of ferrite. Measurements were carried out in two directions determined by the ϕ angle (i.e., for ϕ = 0° and 90°) in the case of the initial sample and then in one direction (i.e., ϕ = 0°) when the tensile load was applied "in situ" along the transverse direction (TD in Fig. 3a). The Set-X diffractometers were used to measure interplanar spacings for the extended range of $\sin^2\Psi$ (0-0.8) and for the negative and positive Ψ angles. As the result, the tensors of phase stresses were determined for the initial sample (see Table 2), while the values of σ_{11}^{ph} phase stress as a function of the Σ_{11} were found assuming σ_{33}^{ph} = 0 [9]. The phase stresses were determined independently for ferrite and austenite in the quenched and aged samples (Fig. 5).

TABLE 2

Initial stresses measured in both phases of the studied samples, assuming σ_{33}^{ph} = 0. Sample orientation is given in Fig. 3a

sample	Phase	σ_{11}^{ph} (MPa)	σ_{22}^{ph} (MPa)
quenched	ferrite	-15	29
	austenite	22	-141
aged	ferrite	-32	64
	austenite	58	-41

Neutron diffraction was used to measure "in situ" the lattice strains in duplex steel under an applied tensile load (G5.2 spectrometer with the ^{3}He position sensitive detector in LLB, Saclay, France). The incident neutron wavelength of 2.87 Å was used to obtain scattering angles from austenite 111 and ferrite 110 peaks at $2\theta \approx 86°$ and $2\theta \approx 90°$, respectively. In each measurement the 10×2×2 mm gauge volume crossing the cylindrical sample was used (Fig. 3b). The scattering vector was aligned in the direction of the applied tensile load (along x_1-TD) using transmission technique to measure interplanar spacings (Fig. 3b). Different tensile strains were applied and subsequently the variations of axial force were measured by a dynamometer. For different values of the applied macrostresses the lattice strains ($< \varepsilon_{11}^{\Sigma} >_{\{hkl\}}^{ph}$) were determined in both phases "ph" (see Fig. 7):

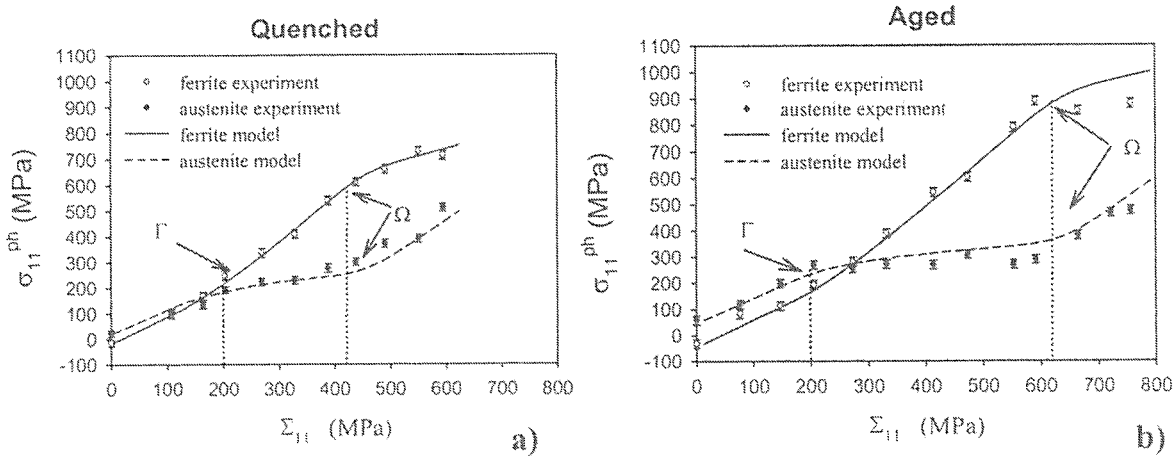

Fig. 5. Phase stresses, corresponding to the applied stress Σ_{11}, measured by X-ray diffraction using 311 reflection ($\lambda_{K\alpha}^{Mn}$ = 0.21035 nm) for austenite and 211 reflection for ferrite ($\lambda_{K\alpha}^{Cr}$ = 0.22911 nm) in quenched (a) and aged (b) steels. The $\sin^2\Psi$ method was used to determine phase stresses from strains measured during "in situ" tensile test (cf. Fig. 3a)

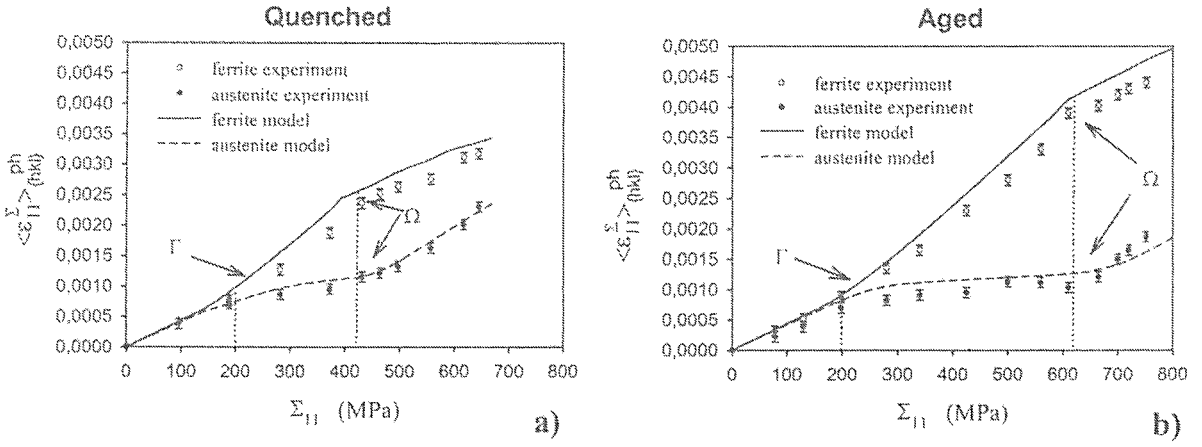

Fig. 6. Elastic lattice strain, corresponding to the applied stress Σ_{11}, measured by neutron diffraction using 111 reflection for austenite and 110 reflection for ferrite in quenched (a) and aged (b) steels. The strains were measured during "in situ" tensile test in the direction of applied stress Σ_{11} (cf. Fig. 3b)

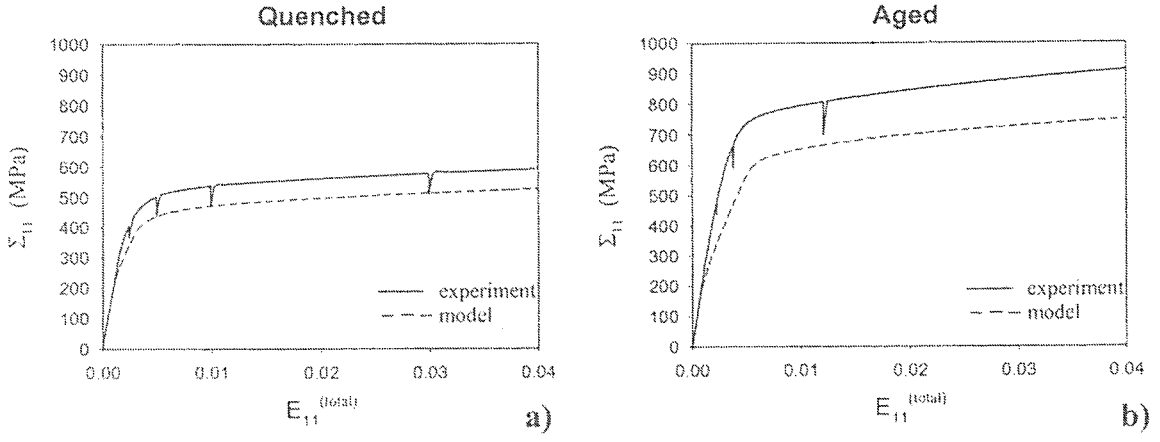

Fig. 7. Results of the mechanical tensile test (solid line) compared with model prediction (dashed line) for quenched (a) and aged (b) steels

$$< \varepsilon_{11}^{\Sigma} >_{\{hkl\}}^{ph} = \frac{< d^{\Sigma} >_{\{hkl\}}^{ph} - < d^{\Sigma=0} >_{\{hkl\}}^{ph}}{< d^{\Sigma=0} >_{\{hkl\}}^{ph}}, \qquad (1)$$

where $< d^{\Sigma=0} >_{\{hkl\}}^{ph}$ and $< d^{\Sigma} >_{\{hkl\}}^{ph}$ are the interplanar spacings measured in x_1 (TD) direction for the non-deformed (reference) sample and for the loaded sample (Σ_{11} is applied), while the brackets denote the average over the volume of diffracting grains belonging to "ph" phase, for which the scattering vector is perpendicular to the {hkl} planes.

In both X-ray and neutron diffraction experiments, the decrease of the load determined at a given (constant) strain was observed in the elastoplastic range of deformation. Thus, the diffraction peaks were measured after stabilisation of the macrostress (Σ_{11}).

The results obtained from diffraction reveal the stress (strain) distribution between phases (ferrite and austenite) of duplex steel. To study the overall properties of the material the mechanical test was performed and the evolution of macroscopic stress (Σ_{11}) vs. macroscopic strain (E_{11}) was determined (Fig. 7). An extensometer was used to determine precisely the macrostrain. The deformation process was stopped at a few points and a decrease and stabilisation of the external load was observed when the applied strain rate was equal to zero (Fig. 7).

4. Interpretation of the results

The experimental points in Fig. 5 illustrate the evolution of the phase stresses σ_{11}^{ph} determined by X-ray diffraction (assuming relaxation of σ_{33}^{ph} component, i.e.,

$\sigma_{33}^{ph} = 0$) as a function of the Σ_{11} stress applied along transverse direction (TD) during the tensile test. It should be noted that in the case of aged sample the α and α' phases are indistinguishable in diffraction and in further study they are treated as one phase (ferrite) having average mechanical properties. Similar evolution of $< \varepsilon_{11}^{\Sigma} >_{\{hkl\}}^{ph}$ lattice strain measured by neutrons in ferrite (i.e., α together with α') and in austenite (γ) is shown in Fig. 6. By analysing the experimental results for both studied samples, it can be shown that at the beginning of loading, the stresses (strains) in both phases were approximately equal to the applied stresses and they change linearly with Σ_{11}. The plastic deformation of austenite starts from a characteristic point (Γ in Figs. 5 and 6) where the load is transferred mostly to the ferritic phase (still elastically deformed). After this point, the stress measured in austenite is lower than that in ferrite and the difference increases with Σ_{11}. The next characteristic point (Ω) shows the elastic limit of ferrite. Starting from this limit, the difference between the phase stresses decreases with an increase of the applied stress (Σ_{11}). The latter evolution indicates that the work hardening of austenite is more significant in comparison with ferrite hardening and the load is now transferred to the austenitic phase [9-11].

The next step of the study was performed by comparing the results of the self-consistent model [28, 29] with experimental data. To predict the elastoplastic process, the calculations were performed for 20000 ellipsoidal inclusions (a/c = 0.1 and b/c = 0.2, where c||RD, b||TD and a||ND) representing grains of austenite (50%) and ferrite (50%). The tensile stress was applied along the transverse direction (TD), i.e., along the b – axis of inclusion. The initial orientations of crystallites, corresponding to the experimental textures (Fig. 4) and initial stresses given in Table 2 were used as the input data for each phase. The elastic behaviour of a grain was characterised by given single crystal elastic constants (i.e., for austenite: C_{11} = 198 GPa, C_{12} = 125 GPa, C_{44} = 122 GPa and for ferrite: C_{11} = 231 GPa, C_{12} = 134 GPa, C_{44} = 116 GPa), however the plastic properties were a priori not known. The calculations were performed assuming that two families of slip systems (i.e., <111>{211} and <111>{110}) for ferrite and one family of slip systems (i.e., <110>{111}) for austenite are active during plastic deformation. Generally, a multi-slip is observed during plastic deformation and in such the case the critical resolved shear stress (τ_c^i) on the system („*i*") depends on shear glides (γ^j) on other active slip systems („*j*"). The linear hardening law was considered and, consequently, the following relation for the rate of critical resolved shear stresses for slip was used:

$$\dot{\tau}_c^i = \sum_j H^{ij} \dot{\gamma}^j \qquad (2)$$

H^{ij} is called the hardening matrix describing the mutual interaction between slip systems [29]. In this work an isotropic hardening is assumed, i.e., all elements of the H_{ij} matrix have the same value H. Moreover, the initial critical resolved shear stress for slip systems belonging to a given family have the same value: τ_c^o.

To determine the elastoplastic parameters of the phases, the model σ_{11}^{ph} stresses were adjusted to those measured by X-ray diffraction. In accord with [9], it was assumed that the σ_{33}^{ph} stresses completely relax (i.e., σ_{33}^{ph} = 0) in the near-surface volume penetrated by X-ray radiation. Similar procedure was applied in the case of neutron diffraction, but in this case the experimental $< \varepsilon_{11} >_{\{hkl\}}^{ph}$ strains were fitted to the model data. As presented in Fig. 5, the theoretical curves agree very well with the experimental points in the elastic range of deformation (below point Γ), i.e., the proper elastic constants were used in modelling as well as in the calculation of the diffraction elastic constants. To adjust the model results to the experimental data in the elastoplastic range (above point Γ), the values of initial critical resolved stress (τ_c^o) were varied for both phases. The first characteristic point (Γ), corresponding to the yield point of the γ-phase, determines the value of τ_c^o for austenite, while the second point (Ω) allows for τ_c^o of ferrite to be found [9-11]. The initial critical resolved shear stress determined for both phases are given in Table 3. By fitting model results to the phase stresses (strains) in the range where both phases are plastically deformed (i.e., above point the Ω), the theoretical ratios of work hardening parameters $H(ferrite)/H(austenite)$ can be found. To find the absolute values of H parameters for each phase, additionally the Σ_{11} vs. E_{11} model functions (where Σ_{11} is the macrostress applied to the sample and E_{11} is the macrostrain measured by strain gauge) must be adjusted to the corresponding experimental values [9-11]. As shown in Fig. 7, the macrostress relaxed slowly to a lower value when the increase of applied strain was stopped. When the tensile test restarted with the same rate, the macrostress rapidly returned to approximately the same value as before relaxation. Consequently, the two different evolutions of Σ_{11} vs. E_{11} were determined in this experiment, i.e., the upper curve in Fig. 7 representing the macrostress which depends on the rate of the applied strain and the lower curve plotted for macrostress values after stabilisation, which illustrates the hardening of the material due to the dislocations multiplication and the intergranular stress presence. The latter plot, describing the state of the material after stabilisation, corresponds to

the conditions occurring during diffraction measurement and it can be related to the Σ_{11} vs. E_{11} dependence predicted by the rate-independent elastoplastic model. Thus, the model results were adjusted to the lower curve shown in Fig. 7 representing the sample after macrostresses stabilisation.

TABLE 3
Plastic deformation parameters determined for quenched and aged steels

	X-ray diffraction		Neutron diffraction	
	quenched DSS	aged DSS	quenched DSS	aged DSS
τ_c^o – ferrite (MPa)	260	370	240	390
τ_c^o – austenite (MPa)	115	110	100	105
H – ferrite (MPa)	80	80	80	100
H – austenite (MPa)	200	245	190	200

The plastic parameters determined for ferrite and austenite in the quenched and aged samples are presented in Table 3. Thermal ageing of the studied austeno-ferritic duplex stainless steel at 400°C during 1000 hours causes a significant increase of the hardness of ferrite (increase of τ_c^o), while the mechanical properties of austenite remained practically unchanged. Finally, the influence of the ageing treatment on the hardness of both phases was confirmed by the Vickers test. The sample surfaces for the Vickers microhardness tests were carried out by mechanical soft polishing followed by a chemical attack (to reveal the phases) and an electro-polishing (to remove the plastically deformed zone). As shown in Fig. 8, a significant increase of hardness of the ferritic phase and unchanged austenite hardness were observed for the aged sample.

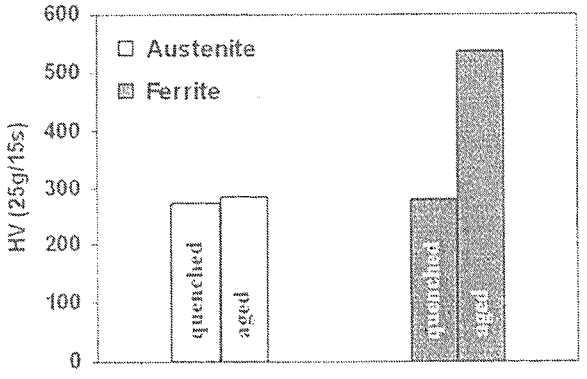

Fig. 8. Microhardness of the austenite and the ferrite phases measured for the quenched and aged steels

Results obtained in this paper confirm the thermal stability of austenite and significant increase of ferrite hardness for the chosen conditions of thermal ageing. Once more the relevance of diffraction methods and the self-consistent modelling in the study of mechanical behaviour of multiphase materials at the phase scale was demonstrated.

5. Conclusions

The main advantage of the diffraction method used in this work was the possibility to separate the measurement of mechanical properties for each phase in multiphase steels. The self-consistent model of elastoplastic deformation was successfully compared with the results of neutron diffraction experiments performed for "in situ" deformed duplex steel. Very good agreement of the measured and the predicted lattice strains was found for the elastic and elastoplastic ranges of deformation. A comparison of experimental and theoretical lattice strains allowed independent determination of the plastic parameters for austenite and ferrite (i.e., τ_c^o, H), characterizing the behaviour of both phases within duplex steel.

It is found that for the quenched duplex steel (without precipitation of secondary phases), the ferritic phase is initially harder than the austenitic phase, i.e. the critical resolved shear stress of ferrite is higher than for austenite. Significant increase of the ferrite hardness was observed after ageing treatment while the mechanical properties of austenite remained unchanged. The results obtained using diffraction were confirmed by the Vickers test, showing a significant increase of microhardnesses of ferrite due to ageing treatment. The evolution of the mechanical properties of duplex steel are caused by the spinodal decomposition of ferrite in α and α' phases accompanied by a precipitation of G phase expected for the chosen conditions of ageing.

Acknowledgements

This research project has been supported by the Polish Ministry of Science and Higher Education (MNiSW) and by the European Network of Excellence: Complex Metallic Alloys (EU 6-th Frame Program). The authors are grateful to the LLB, CEA Saclay (France) for enabling them to use G5.2 spectrometer and to Dr. Vincent Klosek for help during experiment.

REFERENCES

[1] J. O. Nilsson, P. Liu, Mater. Sci. Technol. **7**, 853 (1991).
[2] M. Guttmann, Duplex stainless steel 91, Beaune, France **79** (1991).
[3] A. Mateo, L. Lianes, M. Anglade, A. Redjaimia, G. Metauer, J. Mat.Sci. **32**, 4533 (1997).
[4] C. J. Park, H. S. Kwon, Corrosion science **44**, 177 (2002).

[5] P. Lacombe, B. Baroux, G. Beranger, Les aciers inoxydables, Les éditions de physique, Les Ulis Cedex A, France (1990).
[6] M. J. Marcinkowski, R. M. Fischer, A. Szirmae, Trans. Metall. Soc. AIME **230**, 676 (1964).
[7] R. Lagneborg, Acta Metal. **15**, 1737 (1967).
[8] J. Moverare, M. Oden, Acta Mater. **A337**, 25 (2002).
[9] R. Dakhlaoui, C. Braham, A. Baczmański, Mater Sci and Eng A **444**, 6 (2007).
[10] A. Baczmański, C. Braham, Acta Mater. **52**, 1133 (2004).
[11] R. Dakhlaoui, A. Baczmański, C. Braham, S. Wroński, K. Wierzbanowski, E. Oliver, EC, Acta Mater. **54**, 5027 (2006).
[12] J. Johansson, M. Oden, X.-H. Zeng, Acta Mater. **47**, 2669 (1999).
[13] J. Moverare, M. Oden, Metall. and Mater. Trans. **33A**, 57 (2002).
[14] H. Sidhom, Etude de l'évolution structurale au cours du vieillissement de deux aciers inoxydables austénitiques, et de son influence sur les propriétés mécaniques et de corrosion intergranulaire, These d'état, Université d'Orsay, France (1990).
[15] J. P. Aymard, M. T. Leger, Manuel des aciers moulés, 3e édition, Éditions Techniques des Industries de la Fonderie (1996).
[16] J. P. Massoud, J. C. Van Duysen, G. Zacharie, Thermal ageing of duplex stainless steels, Collection de notes internes de la direction des études et recherches d'EDF, n°93NB00024 (1992).
[17] F. Danoix, S. Chambreland, J. P. Massoud, P. Auger, Évolution microstructurale de la ferrite des aciers austéno-ferritiques lors de vieillissements entre 300 et 400°C, Collection de notes internes de la direction des études et recherches d'EDF, n°92NIB0005 (1991).
[18] P. Berge, G. Zacharie, Endommagement des matériaux dans les centrales nucléaires a eau pressurisée, édition Eyrolles 1997.
[19] V. Calonne, These de doctorat de l'école des mines de Paris: Propagation de fissures par fatigue dans les aciers austéno-ferritiques moulés; influence de la microstructure, du vieillissement et de la température d'essai (2001).
[20] H. Dolle, J. Appl. Cryst., **12**, 489 (1979).
[21] C. M. Brakman, Phil. Mag. A **55**, 39 (1987).
[22] A. Baczmański, K. Wierzbanowski, P. Lipiński, R. D. Helmholdt, G. Ekambaranathan, B. Pathiraj, Phil. Mag. A **69**, 437 (1994).
[23] A. Baczmański, C. Braham, W. Seiler, Phys. Stat. Sol. A **201**, 2886 (2004).
[24] A. Baczmański, C. Braham, W. Seiler, Phil. Mag. **83**, 3225 (2003).
[25] J. S. Kallend, U. F. Koks, A. D. Rollet, H. R. Wenk, Operational Texture Analysis, Raport LA-UR-90-2852, Center for Material Sciences, Los Alamos National Laboratory, USA (1990).
[26] J. H. Bunge, Texture analysis in material science: Mathematical Methods. Butterworths, London (1982).
[27] I. C. Noyan, J. B. Cohen, Residual Streess: New York: Springer Verlag (1987).
[28] P. Lipinski, M. Berveiller, Int. J. of Plasticity **5**, 149 (1989).
[29] P. Zattarin, A. Baczmański, P. Lipinski, K. Wierzbanowski, Arch. Metall. **45**, 163 (2000).

Received: 3 December 2007.